Anomalous quantum oscillations of CeCoIn 5 in high magnetic fields

J. Hornung, S. Mishra, J. Stirnat, M. Raba, B. V Schwarze, J. Klotz, D. Aoki, J. Wosnitza, T. Helm, Ilya Sheikin

Anomalous quantum oscillations of $CeCoIn_5$ in high magnetic fields

J. Hornung,[1,2] S. Mishra,[3,*] J. Stirnat,[1,2] M. Raba,[3,†] B. V. Schwarze,[1,2]
J. Klotz,[1,2] D. Aoki,[4] J. Wosnitza,[1,2] T. Helm,[1,‡] and I. Sheikin[3]

[1] *Hochfeld-Magnetlabor Dresden (HLD-EMFL) and Würzburg-Dresden Cluster of Excellence ct.qmat, Helmholtz-Zentrum Dresden-Rossendorf, 01328 Dresden, Germany*
[2] *Institut für Festkörper- und Materialphysik, Technische Universität Dresden, 01062 Dresden, Germany*
[3] *Laboratoire National des Champs Magnétiques Intenses (LNCMI-EMFL), CNRS, UGA, 38042 Grenoble, France*
[4] *Institute for Materials Research, Tohoku University, Oarai, Ibaraki, 311-1313, Japan*

(Dated: December 3, 2021)

We report on magnetic-torque and resistivity measurements of the heavy-fermion compound $CeCoIn_5$ in static magnetic fields up to 36 T and temperatures down to 50 mK. While quantum oscillations of the de Haas–van Alphen (dHvA) as well as the Shubnikov–de Haas (SdH) effect confirm the previously reported Fermi surfaces, an analysis of the field dependence reveals two anomalous features. The first is seen at about 22 T as a sharp anomaly in the resistivity for current applied along the a direction. The second appears as nonmonotonic field-dependent oscillation frequencies and amplitudes in both dHvA and SdH signals. This second feature emerges at about 28 T. This field is close to that of the nematic transition reported for $CeRhIn_5$ and the proposed Lifshitz transition in $CeIrIn_5$. We discuss possible common grounds of these latter features that might originate from the very similar band structures of these materials.

INTRODUCTION

The Ce-based materials $CeCoIn_5$, $CeRhIn_5$, and $CeIrIn_5$ (or 115 systems for short) have attracted considerable scientific interest. This is caused by the appearance of various exciting phenomena such as heavy-fermion behavior, unconventional superconductivity, quantum criticality, and nematicity [1–10]. The coexistence and similar energy scales of these phenomena render the 115 systems the perfect compounds to investigate the interrelations among these strongly correlated states. On the other side, this diversity makes it challenging to disentangle the various effects for gaining a fundamental understanding. Consequently, there are still many unsolved puzzles in this prototypical class of electronically correlated materials.

One important aspect is the degree of hybridization of the Ce-4f electrons. These electrons possess localized character in $CeRhIn_5$ and itinerant character in $CeIrIn_5$ and $CeCoIn_5$ [11–14]. The degree of hybridization with the conduction electrons can be tuned by external parameters, such as pressure [15], chemical substitution [16–19], and magnetic field [20, 21]. A change of the 4f-electron ground state has a significant impact on the electronic structure and, consequently, on the physical properties.

In $CeRhIn_5$, an anomaly of the resistivity occurs at the onset of a putative electronic nematic phase around 28 T [9, 22]. Interestingly, for $CeIrIn_5$ a similar anomaly appears in the resistivity at nearly the same field value, accompanied by a peak in the thermopower [23, 24]. Motivated by changes in the frequency spectra of the magnetic quantum oscillations, various groups suggested a Fermi-surface reconstruction due to field-enhanced hybridization of the Ce-4f electrons in $CeRhIn_5$ [25–27] and a field-induced Lifshitz transition in $CeIrIn_5$ [24]. Recent investigations, however, have shown that the onset of nematicity and the accompanying anomaly in the resistivity in $CeRhIn_5$ [9, 22] are not connected to a change of the localized character of the Ce-4f electrons [28] and that the high-field and high-pressure regime, though sharing the feature of suppressed magnetism, are not connected by a continuous line in the phase diagram [29].

Since the Ce-4f electrons possess different ground states in $CeRhIn_5$ and $CeIrIn_5$, the high-field anomalies were not related to each other. However, these anomalies may have a common origin, for example, in the similar band structures. This motivated us to conduct a Fermi-surface study of $CeCoIn_5$ up to much higher fields than done before. Unlike for $CeRhIn_5$ and $CeIrIn_5$, for $CeCoIn_5$ there exist quantum-oscillation studies only up to 28 T. Therefore, we performed high-field magnetic-torque and electrical-transport measurements up to 36 T. Hereby, the main focus is laid on the analysis of magnetic quantum oscillations and the evolution of the Fermi surfaces. Indeed, we observed a step-like anomaly in the magnetotransport data at 22 T and anomalous behavior in the quantum-oscillation signals at around 28 T in $CeCoIn_5$ as well.

EXPERIMENTAL

We prepared high-quality single crystals of $CeCoIn_5$ by the In self-flux method, according to the method presented in Ref. [11] and confirmed the crystallinity and quality by Laue diffraction and energy-dispersive x-ray spectroscopy [crystal structure in Fig. 1(a)]. The observation of quantum oscillation further proofs the high quality of our samples. We measured the de Haas–van Alphen (dHvA) effect using a capacitive torque-

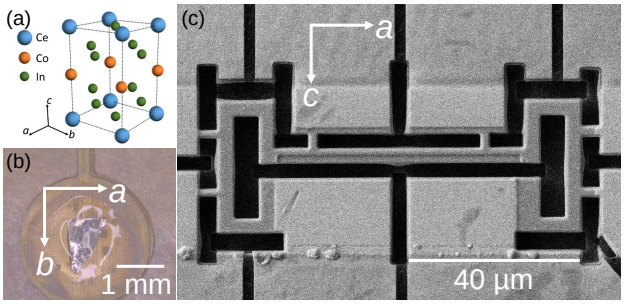

FIG. 1. (a) Crystal structure of $CeCoIn_5$. (b) Picture of the single-crystalline sample fixed to the copper-beryllium cantilever used in the torque experiments. (c) Scanning-electron-microscope image of the measured $CeCoIn_5$ microstructure. We cut the sample, using a focused ion beam, in a way to allow a current flow simultaneously along the crystallographic a and c direction (horizontal and vertical in the image, respectively).

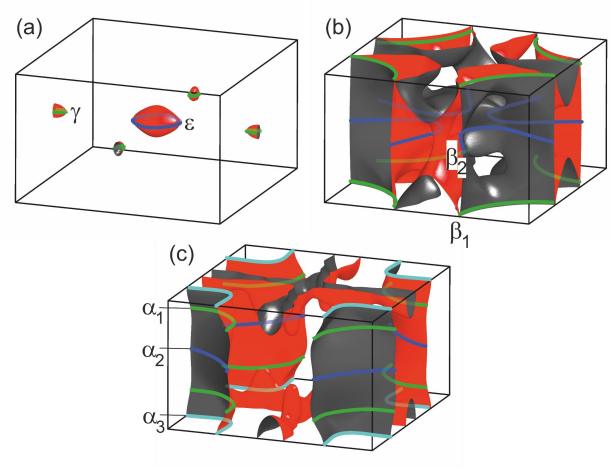

FIG. 2. (a) to (c) Calculated Fermi surfaces for the three bands cutting the Fermi energy. Solid lines and labels highlight selected extremal orbits for $B \parallel c$.

magnetometry method, by utilizing a CuBe cantilever. A sample with a mass of approximately 0.3 mg, was mounted onto a 50 μm thin cantilever and fixed with Apiezon N-grease, as is shown in Fig. 1(b). We recorded the capacitance with a Wheatstone-bridge setup connected to a Stanford SR830 lock-In pre-amplifier.

For the Shubnikov–de Haas (SdH) experiments, we fabricated a microstructure, using a gallium focused-ion-beam system, out of a sample from the same batch of single crystals. With a Ga beam, accelerated by 30 kV, we separated a thin lamella-shaped slice with a thickness of approximately 2 μm from the bulk crystal and structured the slice after being transferred into insulating epoxy. The microstructure, shown in Fig. 1(c), allows us to measure the resistivity of the sample simultaneously along different well-defined crystal axes. We designed the sample geometry in a way that we could measure the resistivity along the crystallographic a and c direction. We realized ohmic contacts by sputter deposition of a 120 nm thick gold film. For further details about the production process, see for example, Ref. [30]. We applied a standard 4-probe lock-In technique for the resistance measurements, applying currents of $10 - 50\,\mu$A in order to prevent overheating effects.

We measured, both the dHvA and SdH effect, in a ^{3}He/^{4}He dilution refrigerator at temperatures down to 50 mK with the sample directly immersed in the mixture and in magnetic fields up to 36 T produced by a resistive magnet at the EMFL facility of the LNCMI in Grenoble. In order to keep eddy current heating effects low the field was ramped with maximum speed of 10-20 mT/s. We used a single-axis rotator that enabled an *in-situ* variation of the sample orientation with respect to the magnetic field.

RESULTS

To set the stage, we show the well-known [11, 14, 31] calculated Fermi surfaces of $CeCoIn_5$ in Fig. 2, reproduced by own band-structure calculations. We have highlighted and labeled selected extremal orbits for magnetic field aligned along the c direction. Panels (a), (b), and (c) show the Fermi surfaces commonly referred to as the γ and ϵ, β, and α sheet, respectively.

While the Fermi-surface morphologies of the sheets of the first band are simple ellipsoids, with extremal orbits γ and ϵ (also called a in Ref. [32] and in the following), the quasi-two-dimensional Fermi surfaces of the β and α sheets are rather complex. For field aligned along c, the extremal orbits β_1 and β_2 as well as α_1 to α_3 appear, respectively.

Magnetic Torque

As an example, we show the background-subtracted torque signal of $CeCoIn_5$ vs. $1/B$ (inset of Fig. 3) together with the fast Fourier transformation (FFT) of the data between 20 and 36 T (main panel of Fig. 3). We subtracted the monotonous background using a low-order polynomial fit. The direction of the magnetic field was tilted by an angle $\Theta = 6°$ from the crystallographic c towards the a axis. We observe clear quantum oscillations composed of various frequencies that comply with predicted orbits (Fig. 2).

In general, we observe very similar quantum-oscillation spectra as reported already before in experiments performed up to 18 T [11, 14, 31]. In order to study the field-dependent evolution of the dHvA oscillations we applied a sliding field-window FFT approach. The window size was kept constant in B^{-1} ($\Delta B^{-1} = 0.009$ T^{-1}).

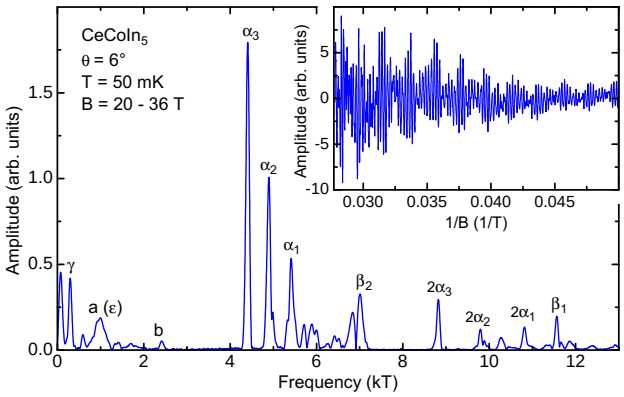

FIG. 3. Fourier transform of exemplary magnetic-torque data measured at $\Theta = 6°$ and shown in the inset versus inverse field after subtraction of a monotonous background. We labeled relevant FFT peaks (see text).

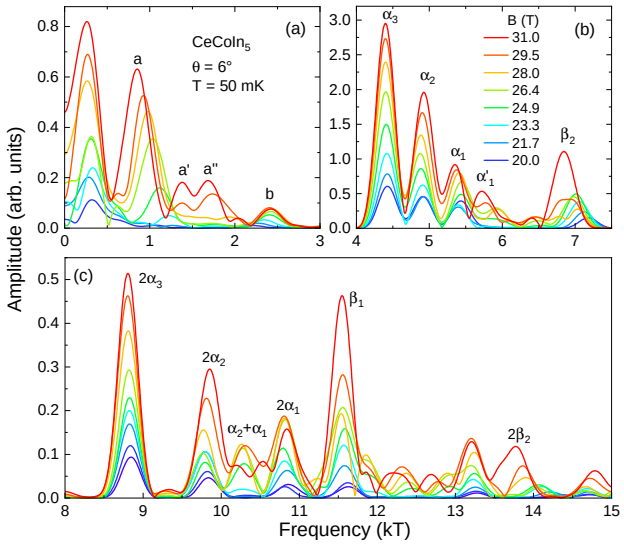

FIG. 4. FFT spectra of the dHvA signal of $CeCoIn_5$ at $\Theta = 6°$ for selected magnetic fields. The three panels, (a), (b), and (c), show excerpts of different frequency ranges. The different colors depict FFT spectra of different overlapping field ranges with same size in B^{-1} ($\Delta B^{-1} = 0.009\ \mathrm{T}^{-1}$) and the harmonic mean given in the legend. Due to the large differences of the amplitudes, we have chosen different ordinates.

Thereby, the width of the analyzed field range is a trade-off between frequency and field resolution. Notably, the amplitude and frequency of a specific quantum oscillation is always the harmonic mean of each FFT field window. We show the corresponding spectra for $\Theta = 6°$ and $T = 50$ mK in Fig. 4. The three panels show excerpts of different frequency ranges. As mentioned, we find the well-known extremal orbits depicted in Fig. 2. Besides that, we observe higher harmonics, possible magnetic-breakdown frequencies (such as α_1'), as well as the frequencies a', a'', and b of unknown origin.

Interestingly, the field dependence of the spectra shows

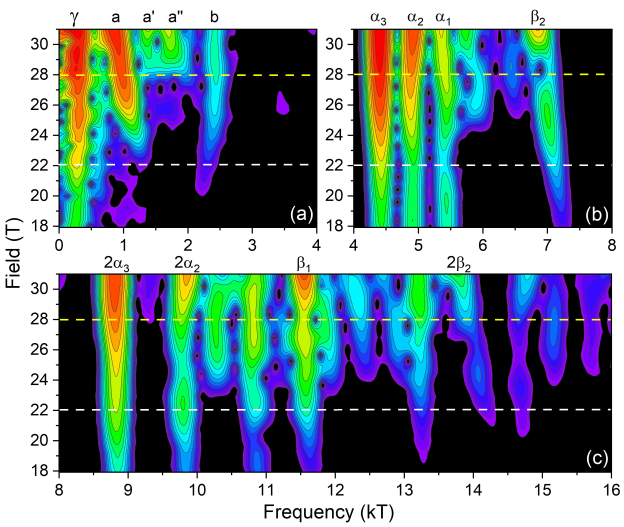

FIG. 5. Contour plot of the field dependence of the dHvA spectra at $\Theta = 6°$ shown in Fig. 4 as line plots. The different colors depict different amplitudes, from low (black) to high (red).

multiple peculiarities, such as nonmonotonous amplitude growths, field-dependent frequencies, splitting of frequencies, and the appearance of additional ones. To better visualize these changes in the dHvA FFT spectra, the data for $\Theta = 6°$ and $\Theta = 4°$ are shown as contour plots in Figs. 5 and 6, respectively. In this way, the y axis represents the field value, while the Fourier-transformation amplitude is encoded in the color.

Our analysis of the field-dependent evolution of the dHvA spectra reveals unusual behavior not expected for metals. For example, some quantum-oscillation frequencies show a continuous shift with increasing field, most pronounced for the β_2 orbit, but also the a and b frequencies change with field. Furthermore, the β_2 amplitude shows a strong suppression and splitting at about 28 T and for $\Theta = 6°$ [Fig. 5(b)]. Around this field, further peculiarities evolve, such as the emergence of two new frequencies of unknown origin, labeled a' and a'', as well as a pronounced suppression of the oscillation amplitudes of β_1, both at 6° and 4° [Figs. 5(c) and 6(c), respectively] and of α_1 at 4° [Fig. 6(b)].

The α_1' as well as the a' and a'' frequencies may arise from magnetic breakdown or magnetic interaction [33] between α_1 (as well as a) and a smaller orbit. Indeed, we observe a broad but pronounced peak, possibly the γ orbit (Fig. 2), at around 300 T [Fig. 4(a)]. We should note, however, that such low frequencies are very sensitive to background subtraction. Therefore, we cannot determine the origin of the above-mentioned frequencies with certainty.

As described by Shoenberg [33], the amplitudes of magnetic-quantum oscillations, in general, depend on various factors, such as the curvature of the Fermi surface

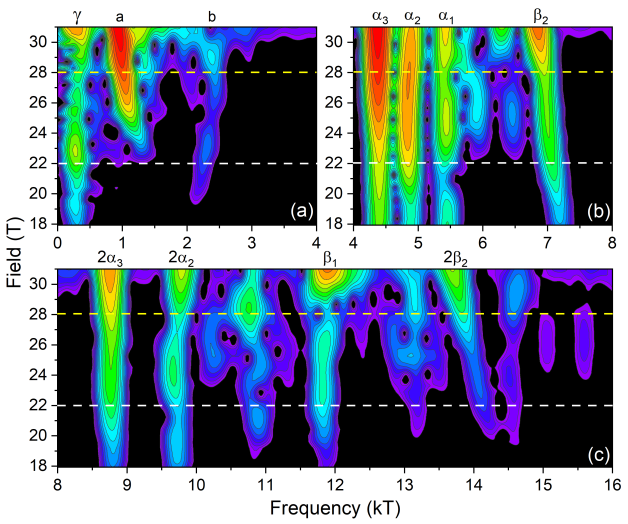

FIG. 6. Contour plot, as explained for Fig. 5, for dHvA data obtained at $\Theta = 4°$.

at the extremal orbits parallel to the magnetic field, the effective masses of the quasiparticles, the mean free path of the charge carriers, and interference and magnetic-breakdown effects. In addition, for dHvA oscillations measured by use of the torque method, the oscillation amplitude depends on the anisotropy of the Fermi surface [33]. Therefore, deviations from the expected exponential field dependence of the quantum-oscillation amplitudes can be caused by a change of any of these parameters.

In the context of heavy-fermion systems, the most prominent of these parameters certainly is the effective mass, m^*, which represents the renormalized band mass; due to many-body interactions, m^* may be enhanced by some 100 times compared to the band mass. The renormalized effective mass can be taken as a measure for the degree of hybridization of the $4f$ electrons. However, other influences (e.g., quantum-critical fluctuations) may increase its value as well.

We extracted the effective masses of various orbits from our torque measurements at 6° between 50 and 450 mK. In Figs. 7(a) and 7(b), we show the frequency spectra for selected temperatures at the highest field range. As an example, Fig. 7(c) shows the temperature-dependent amplitudes of the β_1 orbit for selected fields. The solid lines are fits using the Lifshitz–Kosevich formula [33]. From that, we obtain the field dependence of the effective mass of the β_1 and other orbits, as shown in Fig. 7(d) in units of the free electron mass, m_e. While the authors in a previous work reported spin-dependent effective masses in $CeCoIn_5$ [34], we refrained from using the extended Lifshitz–Kosevich formula for spin-dependent effective masses, due to the large number of additional free parameters. However, for the β_2 orbit around 28 T, the oscillation amplitude gets reduced and two split subfrequencies appear that are shifted to slightly below and above β_2, labeled β_2^l and β_2^h, respectively. For both the resolution was good enough to determine the spin-dependent effective masses directly (see next paragraph). Above 30 T, the amplitudes of the two subfrequencies are too low. Hence, we used the second harmonic, $2\beta_2$, to determine the spin-dependent effective masses.

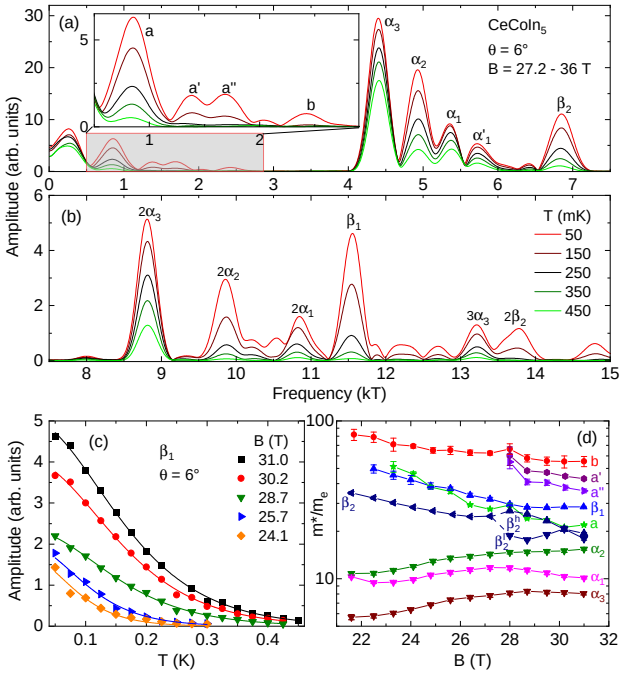

FIG. 7. dHvA spectra of $CeCoIn_5$ from (a) 0 to 7.5 kT and (b) from 7.5 to 15 kT for selected temperatures between 50 and 450 mK at $\Theta = 6°$ and for the harmonic-mean-averaged field of 31.0 T. The inset in (a) shows an enlargement of the marked frequency range. (c) Temperature dependence of the amplitudes of the frequency β_1 for selected field ranges. The solid lines are fits using the Lifshitz–Kosevich formula to extract the effective masses. (d) Field dependence of the effective masses of various dHvA frequencies.

The absolute values of the effective masses at 23.3 T differ by a factor of about 12 and range from 6.1 to $71 m_e$, with the effective masses of the α sheet the lowest (Table I). These values are in reasonable agreement with previously reported values [14, 31, 32]. Indeed, for most orbits m^* decreases with increasing field [Fig. 7(d)]. For heavy-fermion materials, this is a well-known effect and interpreted as an indication of decreasing hybridization [31, 35–38]. Surprisingly, we observe a slight increase of m^* for some α orbits [Fig. 7(d) and Table I], the origin of which is unclear. For the b orbit, we find a slight enhancement of the effective mass around 28 T. Likewise, the effective masses of the a' and a'' orbits seem to show a similar behavior, but appear only above 28 T. Furthermore, the effective masses of the two β_2 sub frequencies, β_2^l and β_2^h, differ by almost 9 free-electron masses.

TABLE I. Experimentally determined dHvA frequencies, F, and effective masses, m^*, at $\Theta = 6^\circ$ for two different magnetic fields.

	23.3 T		31.0 T	
orbit	F (kT)	m^* (m_e)	F (kT)	m^* (m_e)
a	1.21	51.3	0.85	21.9
b	2.35	71.0	2.42	55.4
α_1	5.40	9.5	5.35	10.1
α_2	4.91	11.3	4.93	15.4
α_3	4.42	6.1	4.40	8.0
β_1	11.57	45.4	11.55	28.5
β_2	7.06	30.3	6.84	19.6

Resistivity

Using the microstructure shown in Fig. 1, we measured the field-dependent resistivity of $CeCoIn_5$ for two current directions simultaneously, i.e., for current along the a and c direction. Figures 8(a) and 8(b) show the results, respectively, with field oriented along the c direction ($\Theta = 0^\circ$). The insets show enlargements of the high-field regions, with clear quantum oscillations visible. For both current directions, the resistivity shows a step-like increase at the transition from the superconducting to the normal state around 5 T. After a sharp maximum, the resistivity drops for both current directions. While the resistivity with current and field along c goes trough a very broad minimum with a slight increase towards highest fields, the resistivity with current along a, perpendicular to the field, possesses a narrow minimum at about 9 T, which is followed by a positive slope that ends in a clear step-like feature at about 22 T. Indeed, around this field value, some of us found anomalous features in the Nernst coefficient and dHvA effect as well [32].

When changing the field orientation, the resistivity in the normal state increases with increasing Θ [Figs. 8(c) and 8(d)] The step-like feature for current along a shows a clear shift to higher fields, shown in the inset of Fig. 8(c), where the black dots indicate the maximum in the resistivity. This angular dependence is stronger than given by a simple $1/\cos(\Theta)$ function (red dashed line in the inset).

As mentioned, clear quantum oscillations appear at high fields that are more pronounced for current along a. After subtraction of a smooth background, we analyzed the field dependence of the SdH frequencies in the same way as done for the dHvA oscillations. The upper panels in Fig. 9 show the FFT spectra of the SdH signal for current along c, while the lower panels show the spectra for current along a. For this latter current direction, our sliding FFT analysis was limited by the step-like 22 T feature. Besides the larger SdH oscillation amplitudes observed for current along a (the spectra in Fig. 9 are given in the same arbitrary units), we find an additional Fourier peak around 570 T for current along c, the origin of which is unclear.

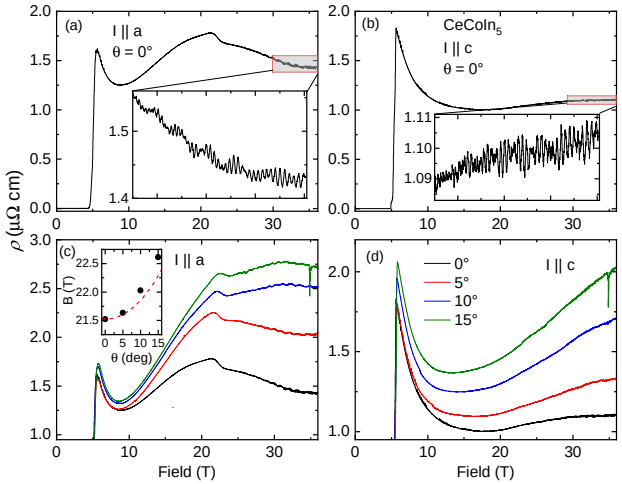

FIG. 8. Field dependence of the resistivity at $\Theta = 0^\circ$ for currents along the (a) a and (b) c axis. (c) Field dependence of the resistivity for current along the a axis and different angles Θ. The inset shows the field dependence of the anomaly. (d) Field dependence of the resistivity for current along the c axis and different Θ. All data were taken at 50 mK.

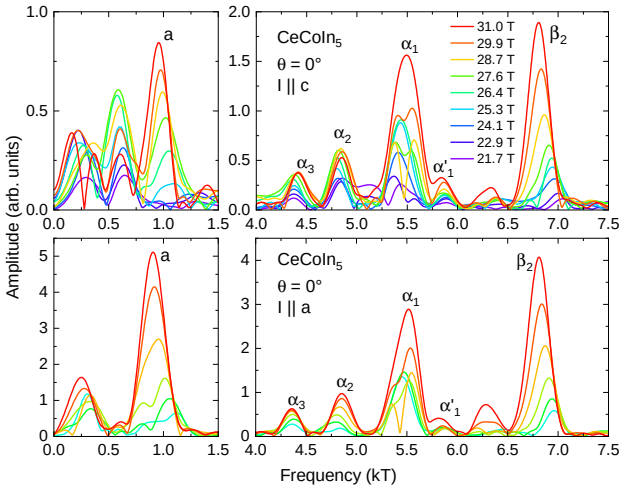

FIG. 9. Fourier spectra of the SdH signals shown in Fig. 8 at various magnetic fields for currents along the c (top) and a direction (bottom).

We observed the three α, the β_2, and the a frequencies in very good agreement with our dHvA results. It is apparent, that the relative amplitudes among the various frequencies differ substantially for the dHvA and SdH oscillations. For example, the three α frequencies show growing amplitudes from α_1 to α_3 in the dHvA effect, while it is vice versa for the SdH effect. This is not unexpected, since the amplitudes of the SdH and dHvA effect are generally not comparable and the magnetic-torque oscillation amplitude depends, in addition, on the Fermi-

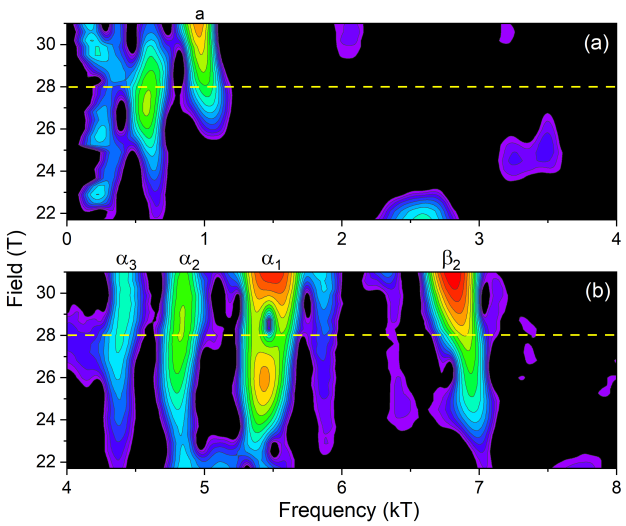

FIG. 10. Contour plot of the field dependence of the SdH spectra shown in Fig. 9 as line plots for current along c.

surface anisotropy.

The field dependence of the SdH amplitudes (see also the contour plot in Fig. 10 for current along c) shows some distinctive features. The β_2 and a FFT peaks exhibit a field-dependent frequency shift, similar as observed for the dHvA data (Figs. 5 and 6). Besides that, some peculiarities appear around 28 T: The amplitude of the α_3 orbit saturates and the amplitude of the α_2 orbit even starts declining (current along c). Another peculiarity is the splitting of the α_1 frequency around 28 T, similar to the splitting of β_2 in the dHvA data for $\theta = 6°$ [see Fig. 4(b)]

DISCUSSION

Our electrical-transport and quantum-oscillation study reveals two anomalous features. First, we observed a distinct step-like anomaly at about 22 T in the in-plane transport for current along the a direction. This supports a previous study that reported evidence for anomalous behavior in the Nernst coefficient and the dHvA amplitudes around 23 T as a consequence of competing energy scales of the Zeeman effect and Kondo interaction [32]. Interestingly, we did not observe any anomaly for current along c. Further, the angular dependence of the step-like anomaly, which increases faster in field than with a simple $1/\cos(\Theta)$ dependence, indicates that it is not the pure out-of-plane component of the magnetic field that drives the transition. Additional work is needed to better understand the origin of this anomaly.

The second feature is the anomalous field dependence of the magnetic quantum oscillations that emerges around 28 T. Both, SdH and dHvA data, show a continuous shift of selected quantum-oscillation frequencies, a

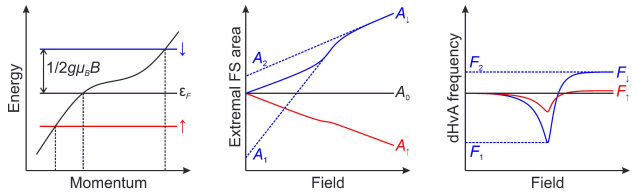

FIG. 11. Schematic sketch of a flattening in the band dispersion (left) and the consequences for the field dependence of the extremal Fermi-surface cross section (center) and the field dependence of the measured dHvA frequencies (right), based loosely on [40]. The position of the anomaly above the Fermi energy is arbitrarily chosen.

splitting of frequencies, and a slight mass enhancement at about this field (as shown for the β_2 orbit). Since we do not observe an abrupt frequency shift in the dHvA and SdH data, a Fermi-surface reconstruction from large to small, caused by a field-induced suppression of the Kondo interaction, as discussed, for example, in URu_2Si_2 and $YbRh_2Si_2$ [20, 21], seems to be very unlikely. For a localization of the Ce-4f electrons more drastic changes of the frequency values and a stronger and more abrupt decrease of the effective masses would be expected [15].

The described anomalies in the quantum-oscillation frequencies can have different reasons. In general, one has to keep in mind, that the spin degeneracy of the electrons is lifted in a magnetic field and the Zeeman effect leads to two spin-split Fermi surfaces with opposite field dependence (left panel of Fig. 11). However, this splitting is not directly observable for a linear correlation between the extremal Fermi-surface area A and the magnetic field. This is due to the fact that the measured frequency $F(B)$ is proportional to the back projection of the field dependent $A(B)$ to zero field, as described by the relation $F(B) \propto A(B) - B\mathrm{d}A(B)/\mathrm{d}B$ [39]. Therefore, the most plausible explanation for the observed sudden splitting of certain frequencies within a narrow field range and the continuous shift with increasing field (both observed for the α_1 and β_2 orbits at certain field orientations) is a nonlinearity in $\mathrm{d}A/\mathrm{d}B$.

Different mechanisms that can cause such a nonlinearity and produce a splitting and field dependence of the observed quantum-oscillation frequencies are illustrated in Ref. [40]. Hereby, a pronounced slope change in the band dispersion, i.e., a sudden band flattening is the most likely scenario. In Fig. 11, we show a qualitative sketch of the described scenario. On the left, we assumed a band dispersion with a flattening above the Fermi energy and indicate the Zeeman-split energies of the spin up and down electrons. This results in a corresponding field dependence of the spin-split extremal Fermi-surface areas (middle panel of Fig. 11) and a concomitant field dependence of the dHvA frequencies (right panel of Fig. 11).

A change of the gradient in the dispersion of one band

would, in the first place, only concern the quantum-oscillation frequencies of one spin-split Fermi surface. But a sudden flattening of the band dispersion would cause a peak in the electronic density of states, that shifts the chemical potential, which, in turn, would lead to anomalies in other frequencies as well [40]. Such a scenario would explain the anomalies we found in the quantum-oscillation signals around 28 T. In addition, it gives a plausible explanation for the appearance of magnetic-breakdown frequencies: The probability of magnetic breakdown strongly depends on the distance of the involved orbits in k space, which changes with the size of the Fermi surface.

Since the band structures of the three Ce-based 115 compounds are very similar, apart from the bands dominated by the $4f$ electrons, the scenario depicted in Fig. 11 could give a common explanation for the anomalies of the quantum oscillations around 28 T, observed here for $CeCoIn_5$ as well as reported for $CeIrIn_5$ [23, 24] and $CeRhIn_5$ [25, 26, 28]. Compared to $CeCoIn_5$, the main difference is, that $CeRhIn_5$ [22] and $CeIrIn_5$ [23] show in addition a clear anomaly in the resistivity at about 28 T. In $CeRhIn_5$, this was identified as a signature of electronic nematicity [9].

A possible scenario to explain the latter effect would be the occurrence of a Pomeranchuck instability [41]. A Pomeranchuck instability, derived from Fermi-liquid theory [42], describes an anisotropic deformation of the Fermi surface caused by strong correlations. Pomeranchuck instabilities are proposed to be the cause for various unconventional phase transitions [43] and the authors of Ref. [44] suggested their possible occurrence in the Ce-based 115 systems. While the mechanism behind the enhancement of the correlations, leading to the Pomeranchuck instability in the 115 systems, remains unclear, an abrupt flattening of the dispersion, as discussed here, would be expected to enhance the electron correlations.

The mechanism behind a field-induced Pomeranchuck instability caused by band-structure anomalies in strongly correlated systems, is described in Ref. [45]. This instability may as well explain the vanishing of quantum-oscillation frequencies and the change from a closed to an open cyclotron orbit [46]. This would provide an explanation for the vanishing of the β_1 orbit in $CeIrIn_5$, reported in Ref. [24]. Very recent specific-heat experiments suggest that the transition to the nematic phase in $CeRhIn_5$ is of weak first order [47], as expected for a Pomeranchuck instability at low temperatures [45]. Additionally, ultrasound measurements revealed a concomitant anomaly, which was interpreted in terms of a metamagnetic transition [48]. While a Pomeranchuck instability is expected to cause anomalies in the sound velocity [49], it may as well influence the magnetic order in antiferromagnetic metals [50] and specifically in heavy-fermion systems [51].

One interesting fact is, that the anomalous behavior in the quantum oscillations around 28 T is accompanied by a similar feature in the resistivity for $CeRhIn_5$ and $CeIrIn_5$, while we did not observe such a feature in $CeCoIn_5$. At first glance, this seems surprising, since $CeCoIn_5$ can be located between the other two 115 systems with regard to the anisotropy and hybridization of the Ce-$4f$ bands. However, as already discussed, not the $4f$ hybridization but the overall band structure plays an important role in this context. Regarding the overall crystal structure and, thus, the overall band structure and density of states, $CeRhIn_5$ and $CeIrIn_5$ have much more in common as compared to $CeCoIn_5$ [52].

SUMMARY

We have performed magnetic-torque and resistivity measurements of the heavy-fermion compound $CeCoIn_5$ in static magnetic fields up to 36 T and temperatures down to 50 mK. Analyses of the field dependence of the dHvA as well as SdH quantum oscillations revealed two anomalous features. First, a step-like anomaly appears in resistivity at about 22 T for current flowing along the a direction, consistent with Nernst and dHvA data reported in Ref. [32].

The second feature manifests at around 28 T leading to various anomalous behavior such as the splitting of quantum-oscillation frequencies, the appearance of new frequencies, and anomalous field dependences of oscillation amplitudes. Here, however, we do not observe any abrupt anomaly in the nonoscillating background signal, neither in magnetic torque nor in resistivity. The field value of the second anomaly is roughly the same as for the putative nematic phase transition observed in $CeRhIn_5$ and the proposed Lifshitz transition in $CeIrIn_5$, which are also accompanied by similar peculiarities in their quantum-oscillation spectra. This suggests a possible common cause based on the very similar band structures of the Ce-based 115 systems. A flattening of the bands close to the Fermi energy would explain the anomalous behavior. This may further lead to a Pomeranchuck instability, which could give rise to the electronic nematicity in $CeRhIn_5$ and the vanishing of the β_1 frequency in $CeIrIn_5$.

ACKNOWLEDGMENTS

We thank A. McCollam and H. Harima for fruitful discussions. The work was supported by the Deutsche Forschungsgemeinschaft (DFG) through the Würzburg-Dresden Cluster of Excellence on Complexity and Topology in Quantum Matter—*ct.qmat* (EXC 2147, Project No. 390858490), by the ANR-DFG under Grant FermiNESt, and by Hochfeld-Magnetlabor Dresden (HLD) at

HZDR and the LNCMI-G, members of the European Magnetic Field Laboratory (EMFL).

* Present address: Los Alamos National Laboratory, Los Alamos, NM 87545, USA
† Present address: IRIG/DEPHY/MEM, CEA-Grenoble, 17 Avenue des Martyrs, 38000 Grenoble, France
‡ t.helm@hzdr.de

[1] P. Gegenwart, Q. Si, and F. Steglich, Nat. Phys. **4**, 186 (2008).
[2] H. v. Löhneysen, A. Rosch, M. Vojta, and P. Wölfle, Rev. Mod. Phys. **79**, 1015 (2007).
[3] G. Knebel, J. Buhot, D. Aoki, G. Lapertot, S. Raymond, E. Ressouche, and J. Flouquet, J. Phys. Soc. Jpn. **80**, SA001 (2011).
[4] S. Wirth and F. Steglich, Nat. Rev. Mater. **1**, 16051 (2016).
[5] C. Petrovic, P. G. Pagliuso, M. F. Hundley, R. Movshovich, J. L. Sarrao, J. D. Thompson, Z. Fisk, and P. Monthoux, J. Phys.: Condens. Matter **13**, L337 (2001).
[6] R. Movshovich, M. Jaime, J. D. Thompson, C. Petrovic, Z. Fisk, P. G. Pagliuso, and J. L. Sarrao, Phys. Rev. Lett. **86**, 5152 (2001).
[7] S. Ikeda, H. Shishido, M. Nakashima, R. Settai, D. Aoki, Y. Haga, H. Harima, Y. Aoki, T. Namiki, H. Sato, and Y. Ōnuki, J. Phys. Soc. Jpn. **70**, 2248 (2001).
[8] J. D. Thompson and Z. Fisk, J. Phys. Soc. Jpn. **81**, 011002 (2012).
[9] F. Ronning, T. Helm, K. R. Shirer, M. D. Bachmann, L. Balicas, M. K. Chan, B. J. Ramshaw, R. D. McDonald, F. F. Balakirev, M. Jaime, E. D. Bauer, and P. J. W. Moll, Nature (London) **548**, 313 (2017).
[10] S. Kirchner, S. Paschen, Q. Chen, S. Wirth, D. Feng, J. D. Thompson, and Q. Si, Rev. Mod. Phys. **92**, 011002 (2020).
[11] H. Shishido, R. Settai, D. Aoki, S. Ikeda, H. Nakawaki, N. Nakamura, T. Iizuka, Y. Inada, K. Sugiyama, T. Takeuchi, K. Kindo, T. C. Kobayashi, Y. Haga, H. Harima, Y. Aoki, T. Namiki, H. Sato, and Y. Ōnuki, J. Phys. Soc. Jpn. **71**, 162 (2002).
[12] D. Hall, E. C. Palm, T. P. Murphy, S. W. Tozer, Z. Fisk, U. Alver, R. G. Goodrich, J. L. Sarrao, P. G. Pagliuso, and T. Ebihara, Phys. Rev. B **64**, 212508 (2001).
[13] S. Elgazzar, I. Opahle, R. Hayn, and P. M. Oppeneer, Phys. Rev. B **69**, 214510 (2004).
[14] A. Polyakov, O. Ignatchik, B. Bergk, K. Götze, A. D. Bianchi, S. Blackburn, B. Prévost, G. Seyfarth, M. Côté, D. Hurt, C. Capan, Z. Fisk, R. G. Goodrich, I. Sheikin, M. Richter, and J. Wosnitza, Phys. Rev. B **85**, 245119 (2012).
[15] H. Shishido, R. Settai, H. Harima, and Y. Ōnuki, J. Phys. Soc. Jpn. **74**, 1103 (2005).
[16] R. Hu, Y. Lee, J. Hudis, V. F. Mitrovic, and C. Petrovic, Phys. Rev. B **77**, 165129 (2008).
[17] K. Chen, F. Strigari, M. Sundermann, Z. Hu, Z. Fisk, E. D. Bauer, P. F. S. Rosa, J. L. Sarrao, J. D. Thompson, J. Herrero-Martin, E. Pellegrin, D. Betto, K. Kummer, A. Tanaka, S. Wirth, and A. Severing, Phys. Rev. B **97**, 045134 (2018).
[18] Q. Y. Chen, F. Ronning, E. D. Bauer, C. H. P. Wen, Y. B. Huang, and D. L. Feng, Phys. Rev. B **100**, 235148 (2019).
[19] D. G. Mazzone, N. Gauthier, D. T. Maimone, R. Yadav, M. Bartkowiak, J. L. Gavilano, S. Raymond, V. Pomjakushin, N. Casati, Z. Revay, G. Lapertot, R. Sibille, and M. Kenzelmann, Phys. Rev. Lett. **123**, 097201 (2019).
[20] K. Sugiyama, H. Fuke, K. Kindo, K. Shimohata, A. A. Menovsky, J. A. Mydosh, and M. Date, J. Phys. Soc. Jpn. **59**, 3331 (1990).
[21] Y. Tokiwa, P. Gegenwart, T. Radu, J. Ferstl, G. Sparn, C. Geibel, and F. Steglich, Phys. Rev. Lett. **94**, 226402 (2005).
[22] P. J. W. Moll, B. Zeng, L. Balicas, S. Galeski, F. F. Balakirev, E. D. Bauer, and F. Ronning, Nat. Commun. **6**, 6663 (2015).
[23] C. Capan, L. Balicas, T. P. Murphy, E. C. Palm, R. Movshovich, D. Hall, S. W. Tozer, M. F. Hundley, E. D. Bauer, J. D. Thompson, J. L. Sarrao, J. F. DiTusa, R. G. Goodrich, and Z. Fisk, Phys. Rev. B **80**, 094518 (2009).
[24] D. Aoki, G. Seyfarth, A. Pourret, A. Gourgout, A. McCollam, J. A. N. Bruin, Y. Krupko, and I. Sheikin, Phys. Rev. Lett. **116**, 037202 (2016).
[25] L. Jiao, Y. Chen, Y. Kohama, D. Graf, E. D. Bauer, J. Singleton, J.-X. Zhu, Z. Weng, G. Pang, T. Shang, J. Zhang, H.-O. Lee, T. Park, M. Jaime, J. D. Thompson, F. Steglich, Q. Si, and H. Q. Yuan, Proc. Natl. Acad. Sci. U.S.A. **112**, 673 (2015).
[26] L. Jiao, Z. F. Weng, M. Smidman, D. Graf, J. Singleton, E. D. Bauer, J. D. Thompson, and H. Q. Yuan, Philos. Mag. **97**, 3446 (2017).
[27] P. F. S. Rosa, S. M. Thomas, F. F. Balakirev, E. D. Bauer, R. M. Fernandes, J. D. Thompson, F. Ronning, and M. Jaime, Phys. Rev. Lett. **122**, 016402 (2019).
[28] S. Mishra, J. Hornung, M. Raba, J. Klotz, T. Förster, H. Harima, D. Aoki, J. Wosnitza, A. McCollam, and I. Sheikin, Phys. Rev. Lett. **126**, 016403 (2021).
[29] T. Helm, A. D. Grockowiak, F. F. Balakirev, J. Singleton, J. B. Betts, K. R. Shirer, M. König, T. Förster, E. D. Bauer, F. Ronning, S. W. Tozer, and P. J. W. Moll, Nat. Commun. **11**, 3482 (2020).
[30] P. J. Moll, Annu. Rev. Condens. Matter Phys. **9**, 147 (2018).
[31] R. Settai, H. Shishido, S. Ikeda, Y. Murakawa, M. Nakashima, D. Aoki, Y. Haga, H. Harima, and Y. Onuki, J. Phys.: Condens. Matter **13**, L627 (2001).
[32] I. Sheikin, H. Jin, R. Bel, K. Behnia, C. Proust, J. Flouquet, Y. Matsuda, D. Aoki, and Y. Ōnuki, Phys. Rev. Lett. **96**, 077207 (2006).
[33] D. Shoenberg, *Magnetic Oscillations in Metals* (Cambridge University Press, Cambridge, UK, 1984).
[34] A. McCollam, S. R. Julian, P. M. C. Rourke, D. Aoki, and J. Flouquet, Phys. Rev. Lett. **94**, 186401 (2005).
[35] W. Joss, J. M. van Ruitenbeek, G. W. Crabtree, J. L. Tholence, A. P. J. van Deursen, and Z. Fisk, Phys. Rev. Lett. **59**, 1609 (1987).
[36] N. Harrison, P. Meeson, P. A. Probst, and M. Springford, J. Phys.: Condens. Matter **5**, 7435 (1993).
[37] E. Haanappel, L. Pricopi, A. Demuer, and P. Lejay, Physica B **259-261**, 1081 (1999).
[38] L. Pricopi, E. Haanappel, S. Askénazy, N. Harrison, M. Bennett, P. Lejay, A. Demuer, and G. Lapertot, Physica B **294-295**, 276 (2001).

[39] J. M. v. Ruitenbeek, W. A. Verhoef, P. G. Mattocks, A. E. Dixon, A. P. J. v. Deursen, and A. R. d. Vroomen, J. Phys. F: Met. Phys. **12**, 2919 (1982).
[40] J.-F. Mercure, S. K. Goh, E. C. T. O'Farrell, R. S. Perry, M. L. Sutherland, A. W. Rost, S. A. Grigera, R. A. Borzi, P. Gegenwart, and A. P. Mackenzie, Phys. Rev. Lett. **103**, 176401 (2009).
[41] W. Metzner, D. Rohe, and S. Andergassen, Phys. Rev. Lett. **91**, 066402 (2003).
[42] I. Pomeranchuk, Soviet Physics JETP **35**, 524 (1958).
[43] J. Quintanilla and A. J. Schofield, Phys. Rev. B **74**, 115126 (2006).
[44] J. C. S. Davis and D.-H. Lee, Proc. Natl. Acad. Sci. U.S.A. **110**, 17623 (2013).
[45] H. Yamase, Phys. Rev. B **76**, 155117 (2007).
[46] C. J. Halboth and W. Metzner, Phys. Rev. Lett. **85**, 5162 (2000).
[47] S. Mishra, A. Demuer, D. Aoki, and I. Sheikin, Phys. Rev. B **103**, 045110 (2021).
[48] S. Mishra, D. Gorbunov, D. J. Campbell, D. LeBoeuf, J. Hornung, J. Klotz, S. Zherlitsyn, H. Harima, J. Wosnitza, D. Aoki, A. McCollam, and I. Sheikin, Phys. Rev. B **103**, 165124 (2021).
[49] H. Adachi and M. Sigrist, Phys. Rev. B **80**, 155123 (2009).
[50] K.-H. Ahn, A. Hariki, K.-W. Lee, and J. Kuneš, Phys. Rev. B **99**, 184432 (2019).
[51] L. P. Gor'kov and A. Sokol, Phys. Rev. Lett. **69**, 2586 (1992).
[52] K. Haule, C.-H. Yee, and K. Kim, Phys. Rev. B **81**, 195107 (2010).